Electronic Supplementary Material (ESI) for Biomaterials Science.
This journal is © The Royal Society of Chemistry 2022

Supporting Information

A multifunctional theranostics nanosystem featuring self-assembly of alcohol-abuse drug and photosensitizers for synergistic cancer therapy

Affiliations: 1. Fujian Provincial Key Laboratory of Cancer Metastasis Chemoprevention and Chemotherapy, College of Chemistry, Fuzhou University, Fuzhou 350116, China.

*** Corresponding author**: Jing-Wei Shao

E-mail addresses: shaojw12@163.com (J.W. Shao)

Telephone: +86-591-22867183

Table S1. The preliminary optimal experiment in G0 and DSF.

Feeding ratio/G0: DSF	Size/nm	Zeta Potential/mV
20 : 1	365.9 ± 10.42	-6.73 ± 1.11
20 : 2	217.4 ± 17.87	2.25 ± 0.55
20 : 3	302.9 ± 25.01	8.18 ± 3.47
20 : 4	224.1 ± 6.63	-7.5 ± 1.24

Table S2. The optimal experiment among G0, DSF and ICG.

Feeding ratio/G0: DSF: ICG	Size/nm	Zeta Potential/mV
20: 4: 0.5	1126 ± 78.07	10.2 ± 3.23
20: 4: 1	149.5 ± 9.85	9.75 ± 2.02
20: 4: 1.5	324.6 ± 10.35	19.6 ± 7.37
20: 4: 2	1105 ± 92.43	9.0 ± 2.89

Table S3. The cytotoxicity assay result in HeLa, HepG2 and SMMC7721 cell lines.

	HeLa		**HepG2**		**SMMC7721**		**H22**	
	IC_{50} (μg/mL)	CI	IC_{50} (μg/mL)	CI	IC_{50} (μg/mL)	CI	IC_{50} (μg/mL)	CI
DSF	11.21		16.08		15.8		21.15	
ICG+NIR	15.06		17.73		16.68		14.38	
DIAGL NPs	8.48	0.58	4.96	0.29	8.81	0.45	5.01	0.35

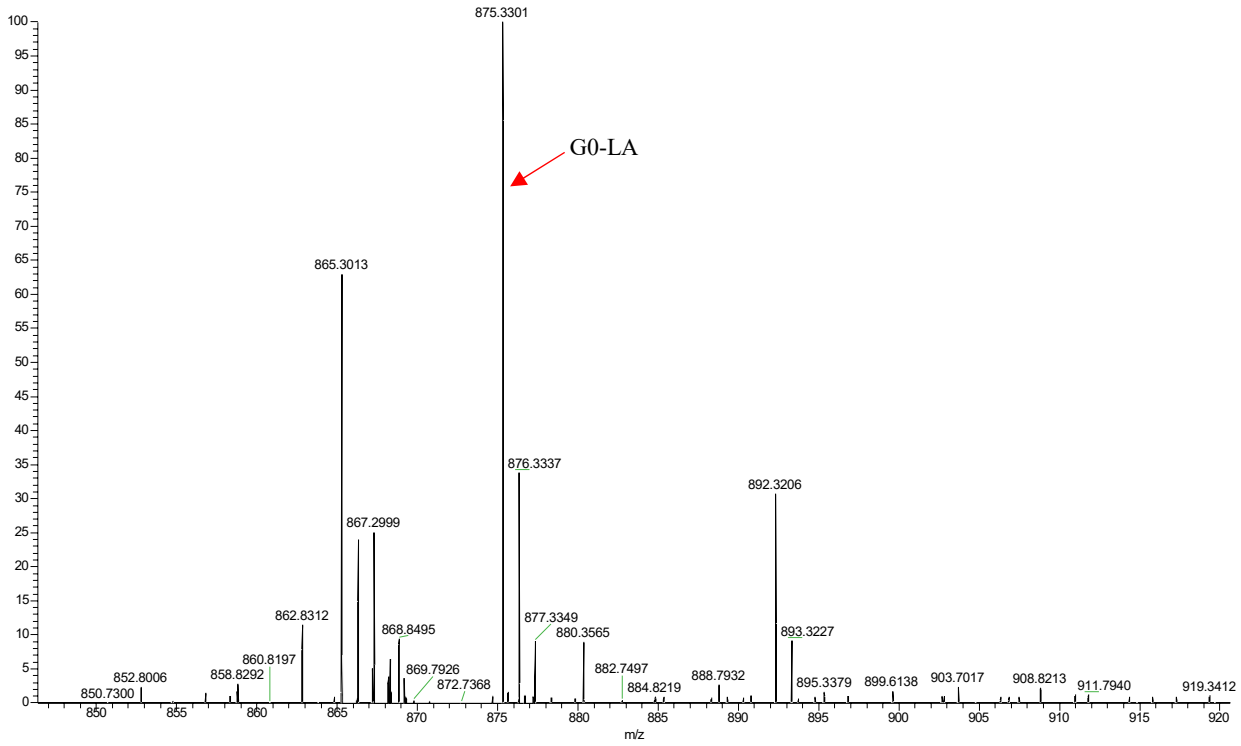

Fig. S1. Mass spectrum of G0-LA.

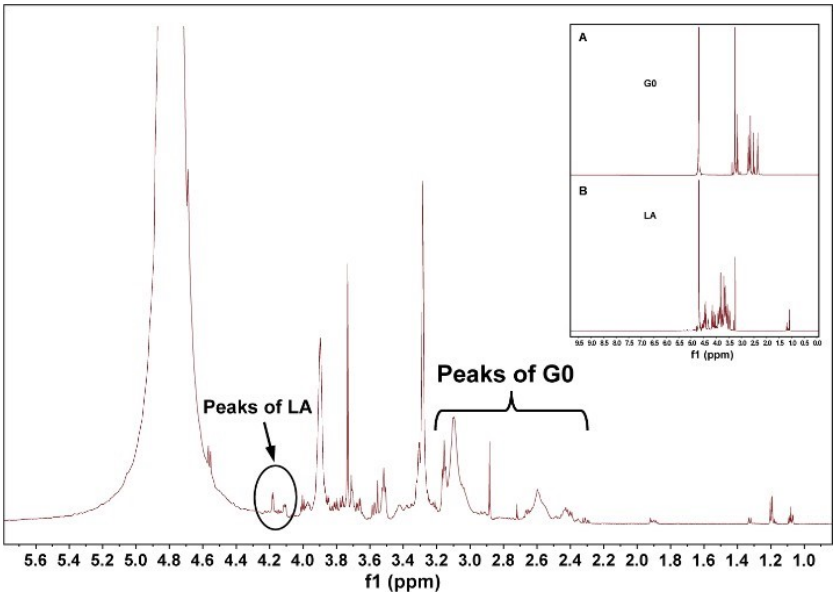

Fig. S2. ^{1}HNMR spectrum of G0, LA and G0-LA.

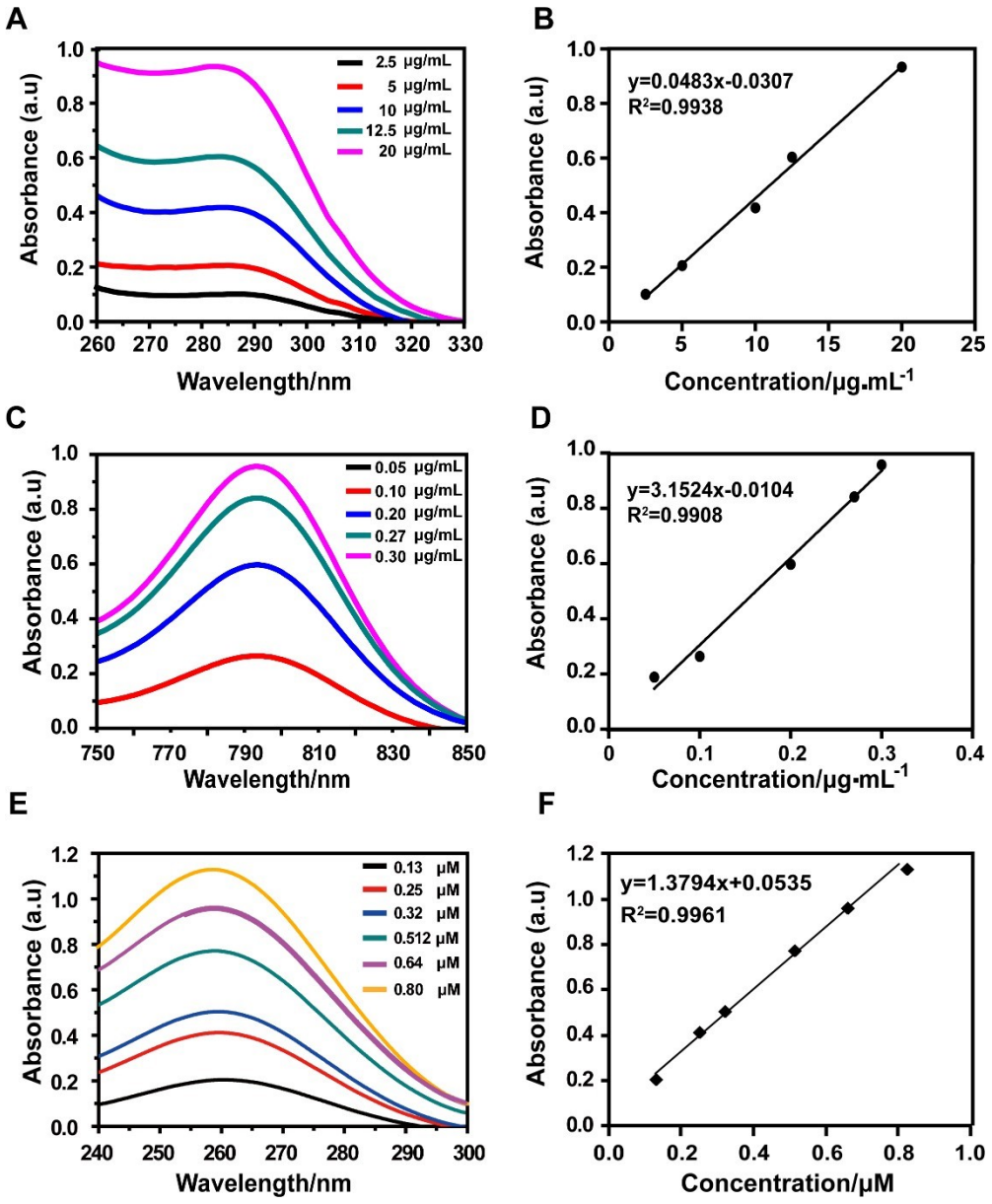

Fig. S3. (A) UV-Vis absorbance spectrum of DSF. (B) The standard curve of DSF. (C) UV-Vis absorbance spectrum of ICG. (D) The standard curve of ICG. (E) UV-Vis absorbance spectrum of aptamer. (F) The standard curve of aptamer.

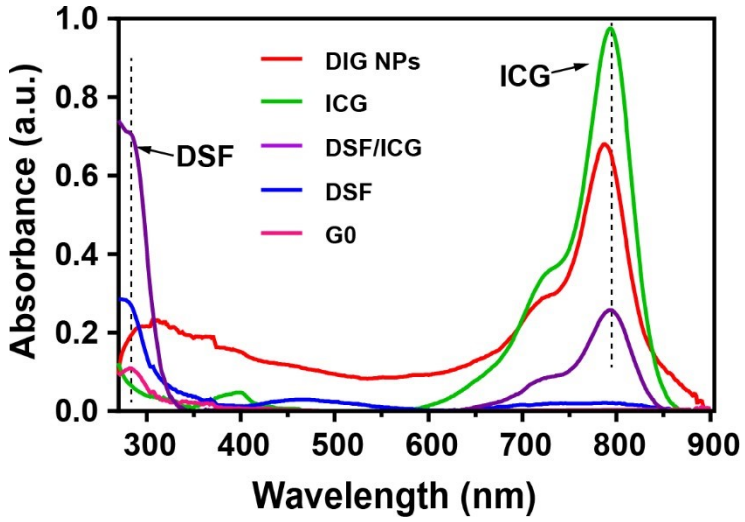

Fig. S4. UV-Vis absorbance spectrum of DSF, G0, ICG, DSF + ICG and DIG NPs.

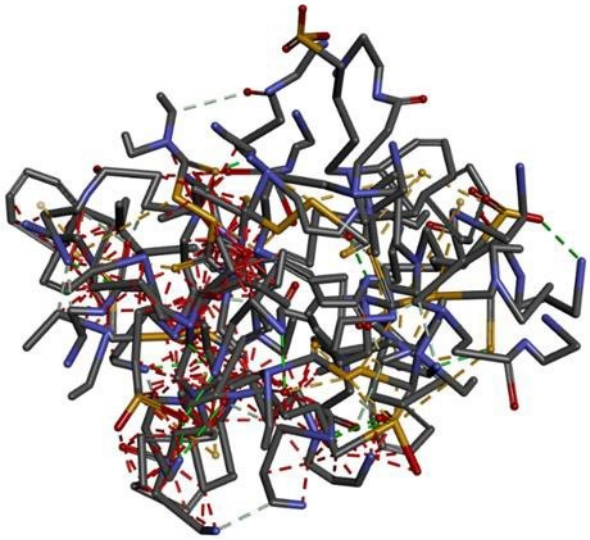

Fig. S5. The molecular simulation DIAGL NPs was opetated by using Discovery Studio 4.5.

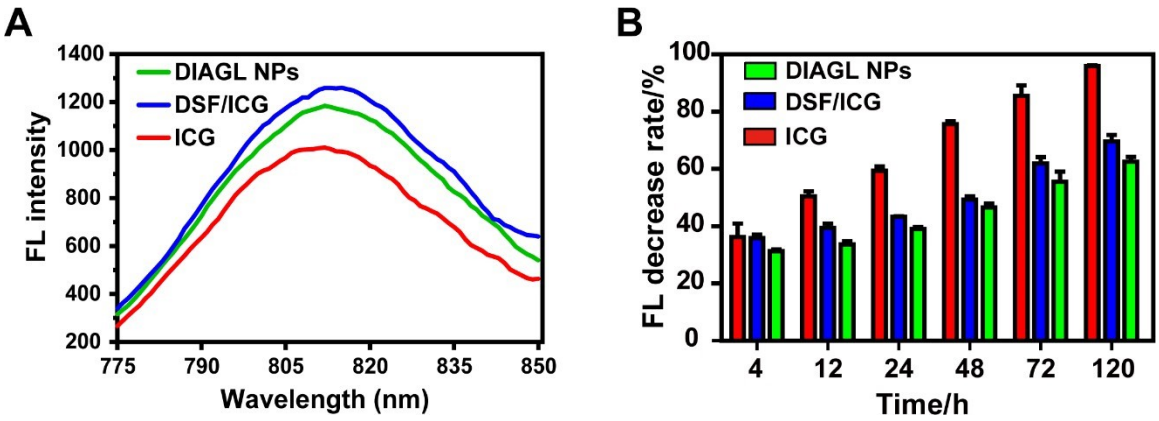

Fig. S6. (A) The fluorescence curve of ICG, DSF/ICG and DIAGL. (B) Quantitative analysis of fluorescence intensity attenuation rate-time changes of ICG, DSF/ICG and DIAGL NPs.

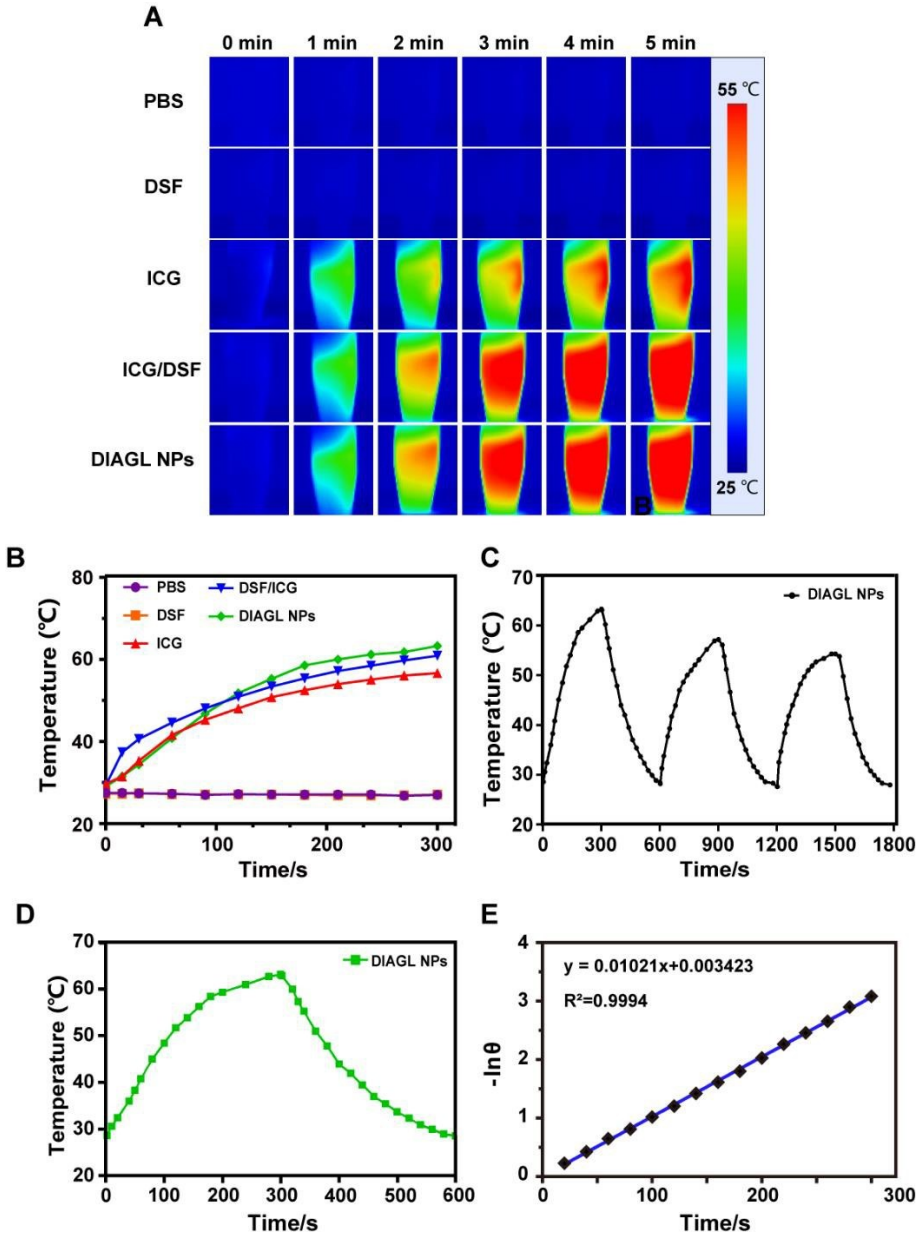

Fig. S7. *In vitro* photothermal effect of DIAGL NPs. (A) Infrared thermographic images and (B) Corresponding photothermic effect curves of PBS, free ICG, ICG/DSF, and DI@AGL NPs. (C) Temperature changes of DIAGL NPs under 808 nm irradiation for 3 cycles. (D) Photothermal effect of DIAGL NPs during one irradiation cycle. The laser was switched off after irradiation for 300 seconds. (E) Fitting the linear relationship between the cooling period and the negative natural logarithm of the temperature.

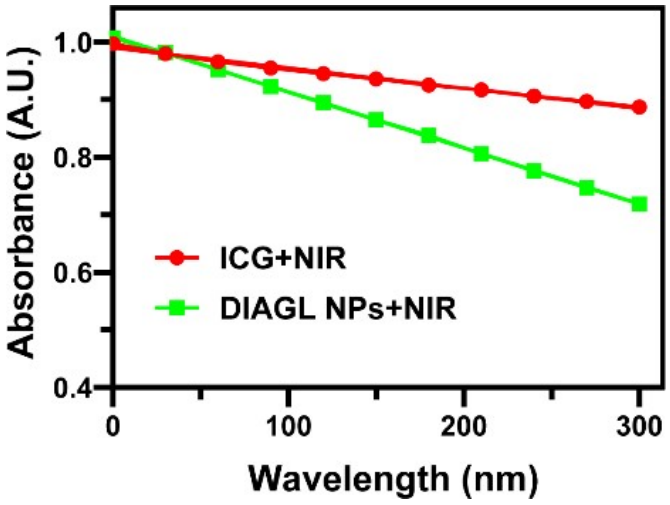

Fig. S8. The singlet oxygen yield study.

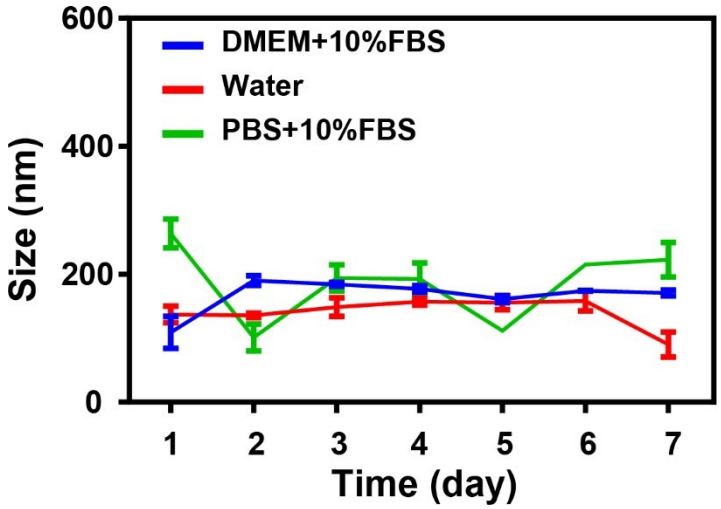

Fig. S9. *In vitro* stability study.

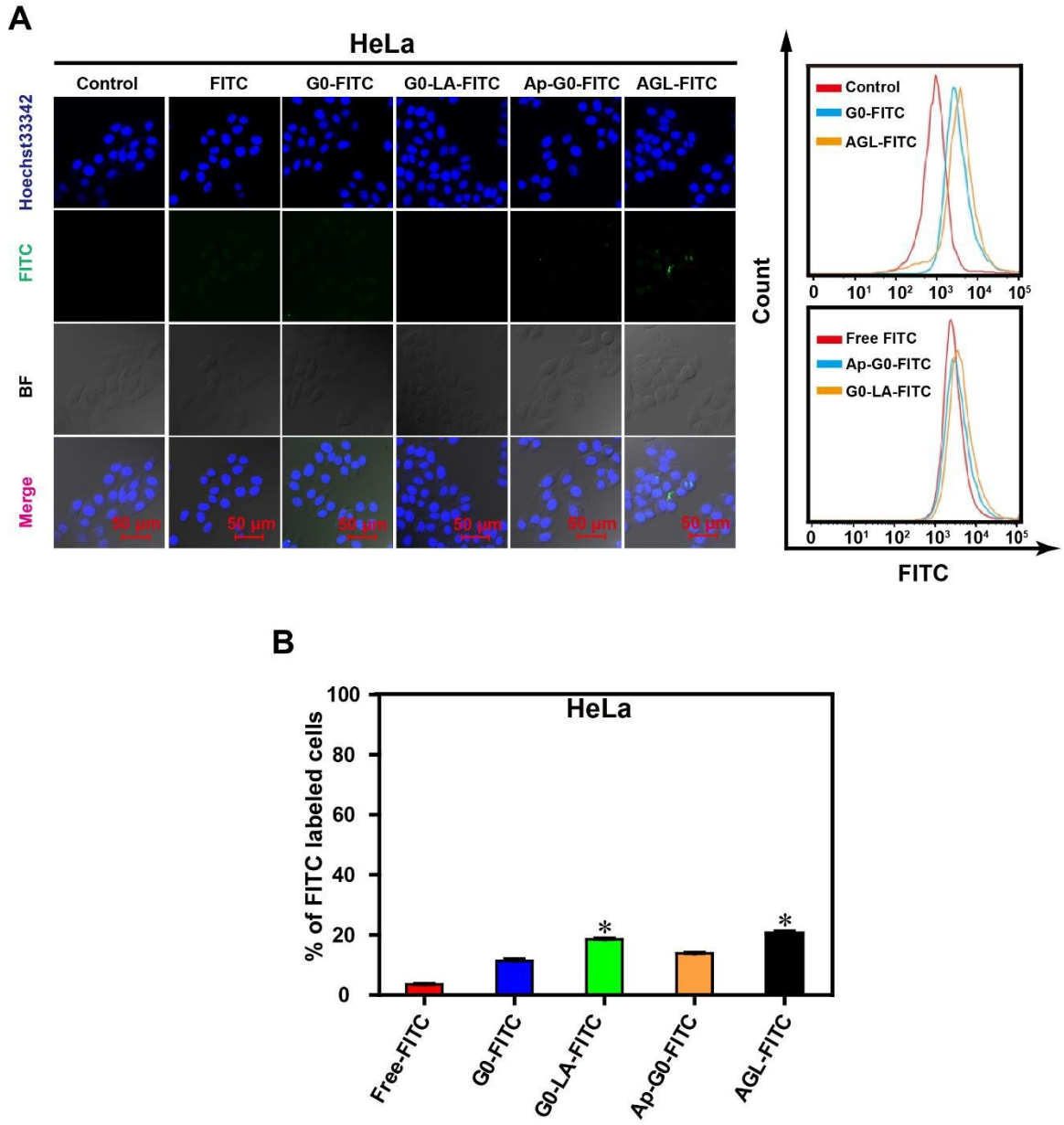

Fig. S10. Confocal images of free FITC, G0, G0-LA, Ap-G0 and AGL for HeLa cells. Blue represented Hoechst 33342 and green represented FITC. Values represented were means ± SD. *p < 0.05, **p < 0.01, ***p < 0.001.

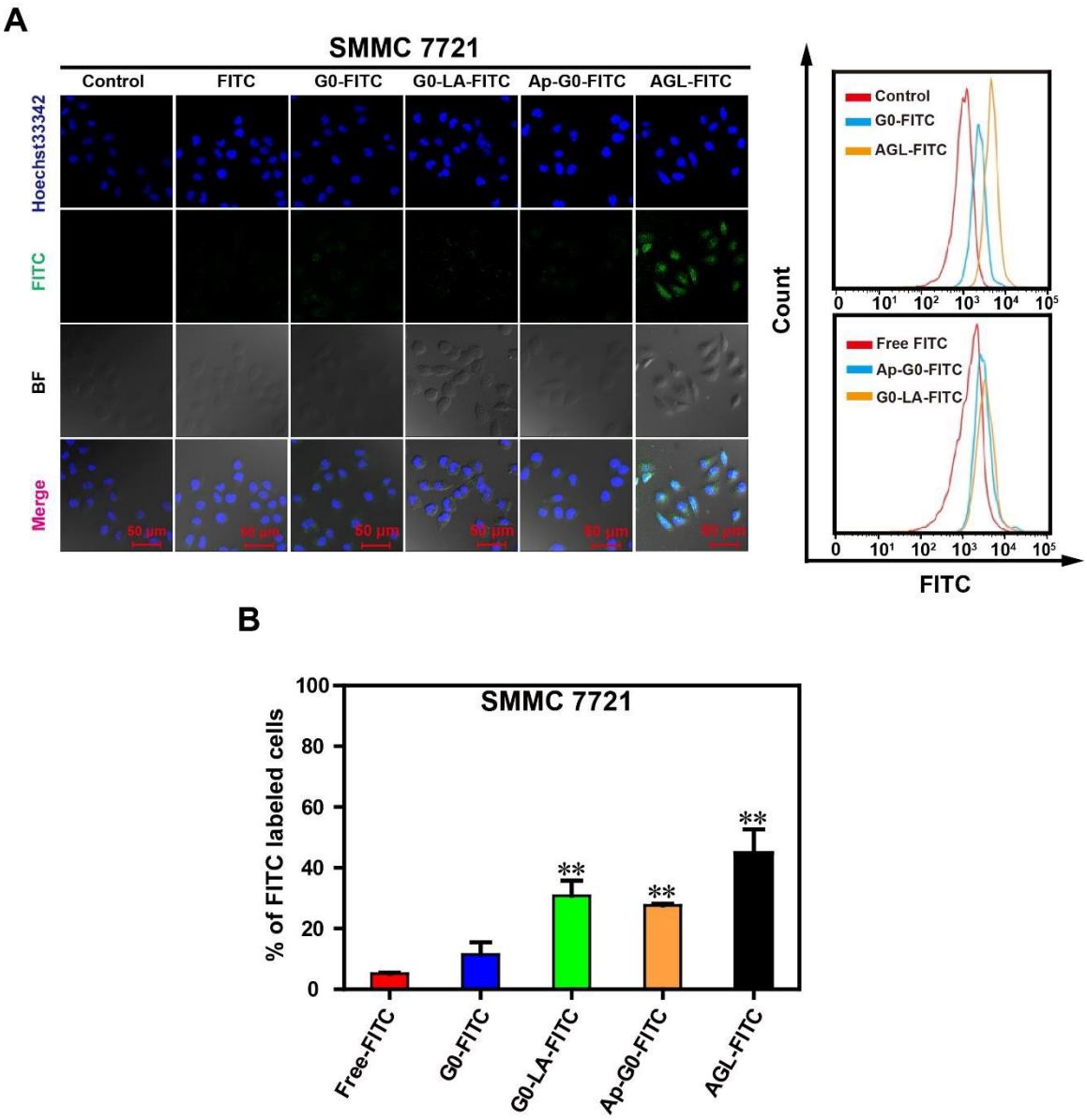

Fig. S11. Confocal images of free FITC, G0, G0-LA, Ap-G0 and AGL for SMMC 7721 cells. Blue represented Hoechst 33342 and green represented FITC. Values represented were means ± SD. *$p < 0.05$, **$p < 0.01$, ***$p < 0.001$.

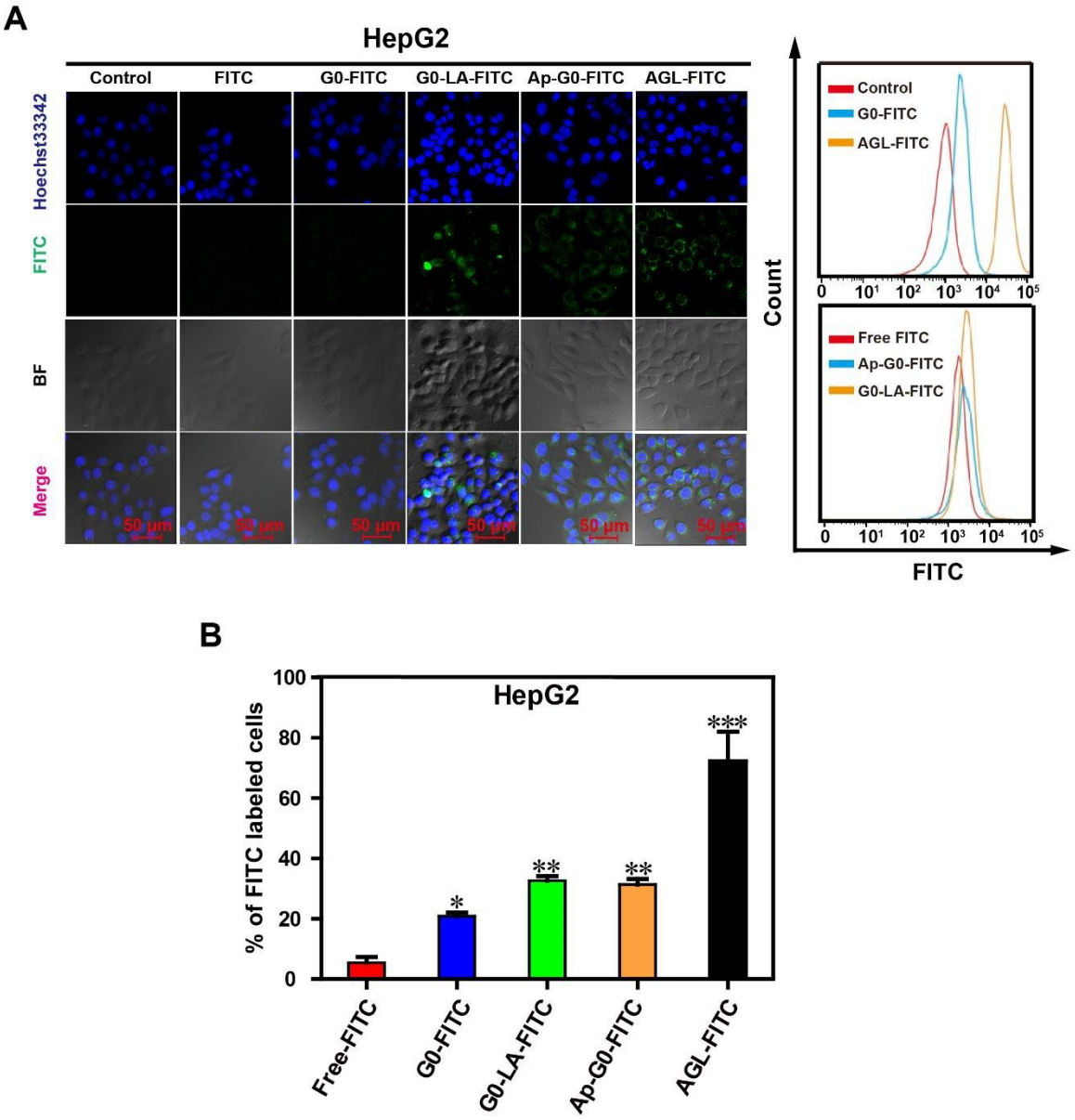

67

68 **Fig. S12.** Confocal images of G0, G0-LA, Ap-G0 and free ICG for HepG2 cells. Blue

69 represented Hoechst 33342 and green represented FITC. Values represented were means ±

70 SD. *$p < 0.05$, **$p < 0.01$, ***$p < 0.001$.

71

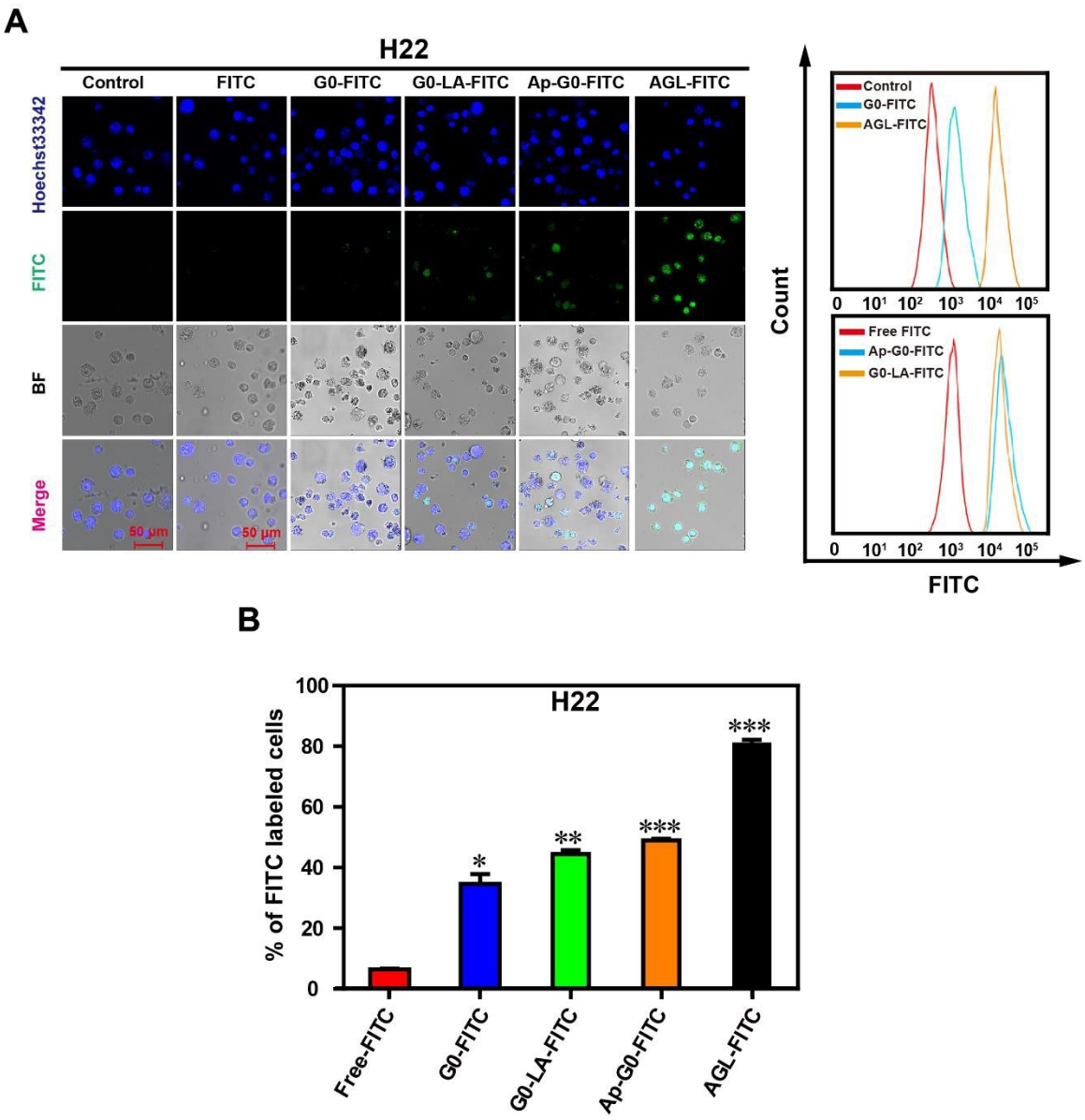

Fig. S13. Confocal images of G0, G0-LA, Ap-G0 and free ICG for H22 cells. Blue represented Hoechst 33342 and green represented FITC. Values represented were means ± SD. *$p < 0.05$, **$p < 0.01$, ***$p < 0.001$.

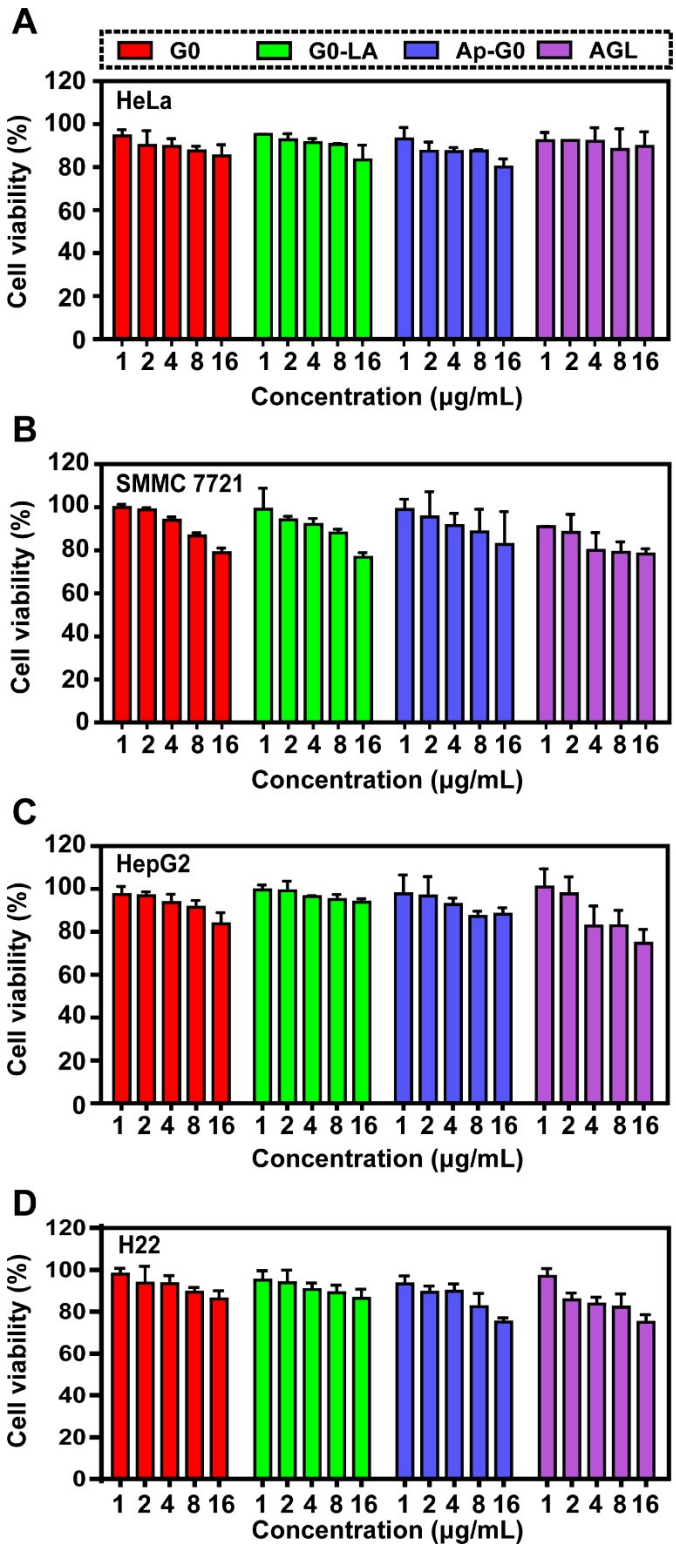

Fig. S14. Evaluation of the cytotoxicity experiment in nanocarrier.

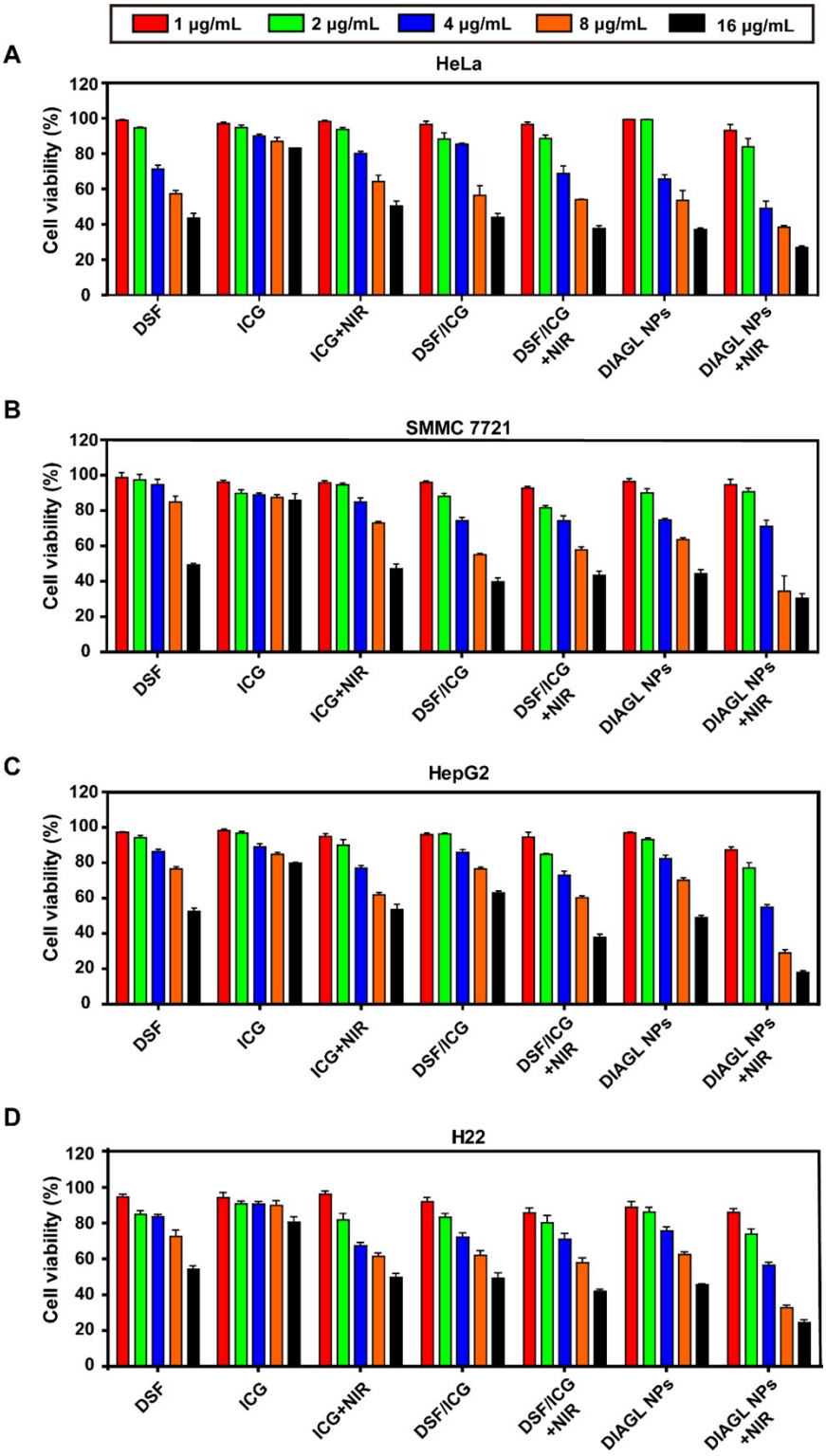

80

81 **Fig. S15.** Evaluation of the cytotoxicity experiment in HeLa, SMMC 7721and HepG2.

82

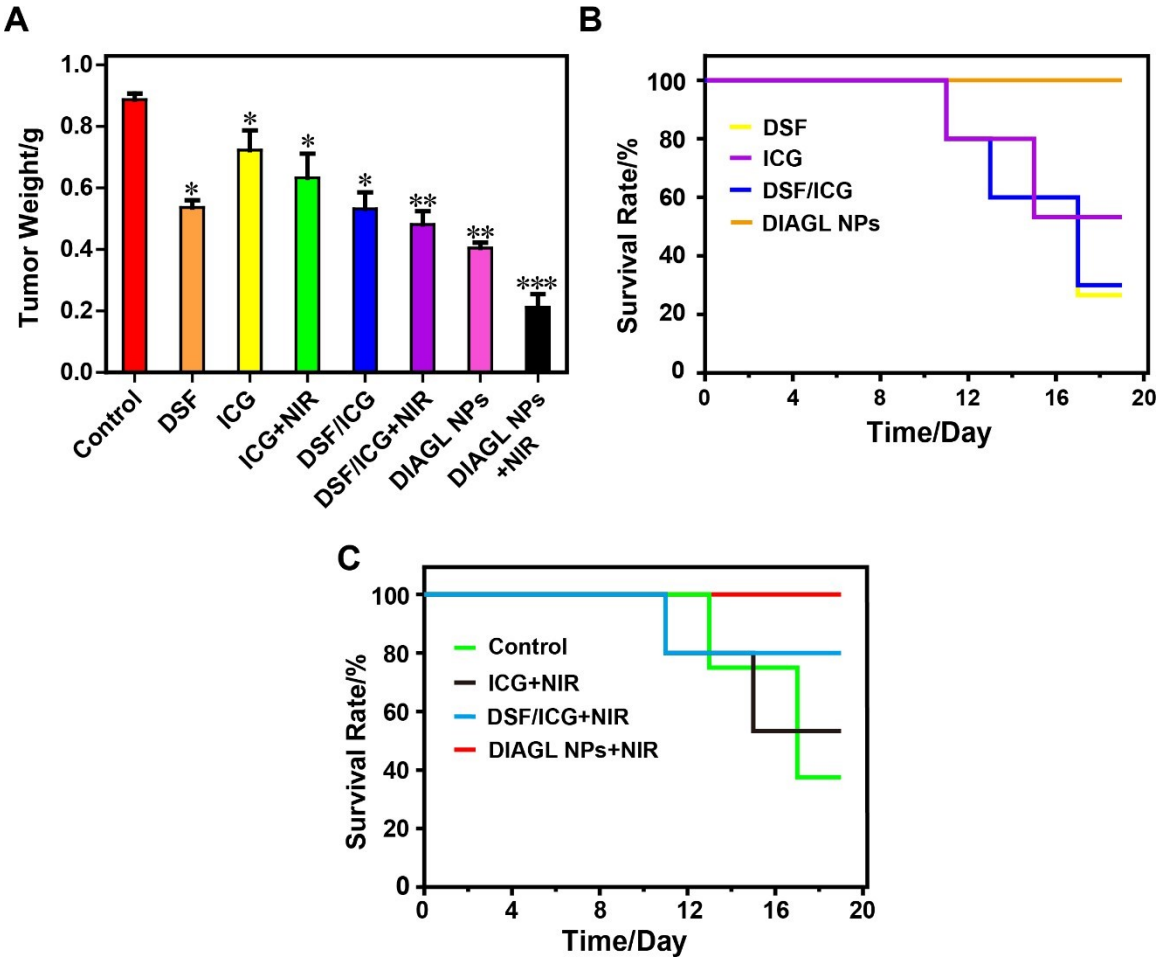

Fig. S16. *In vivo* antitumor effect. (A) Tumor weight change after treatment. (B) and (C) Survival rates of tumor-bearing mice after different treatment. (D) were means ± SD. *p < 0.05, **p < 0.01, ***p < 0.001.

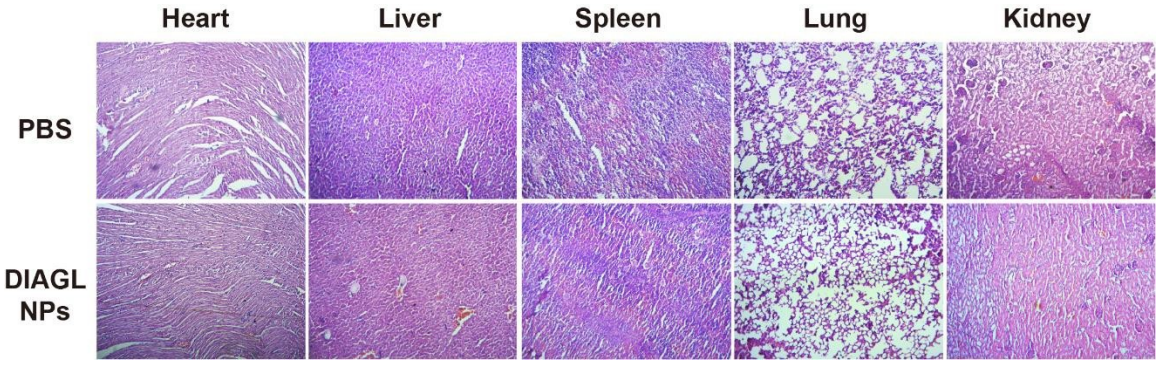

Fig. S17. Hematoxylin-eosin stained histological images obtained from normal tissues including heart, liver, spleen, lung and kidney of H22 tumor-bearing mice after PBS and DIAGL NPs treatment.

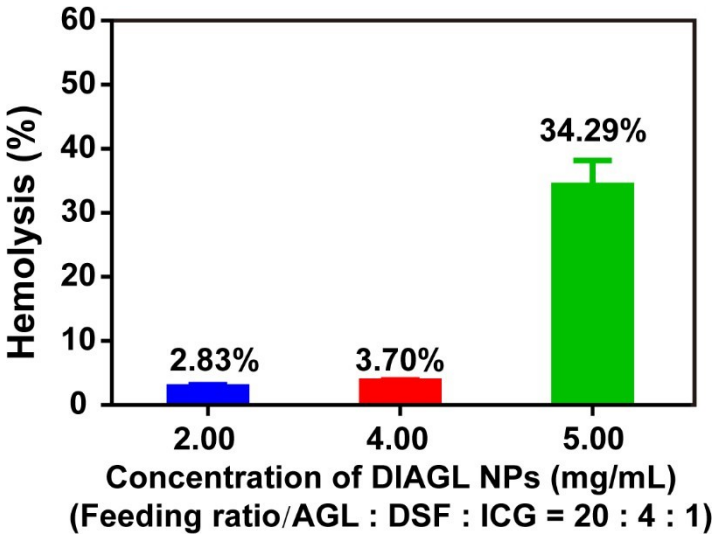

Fig. S18. Hemolytic assay for DIAGL NPs

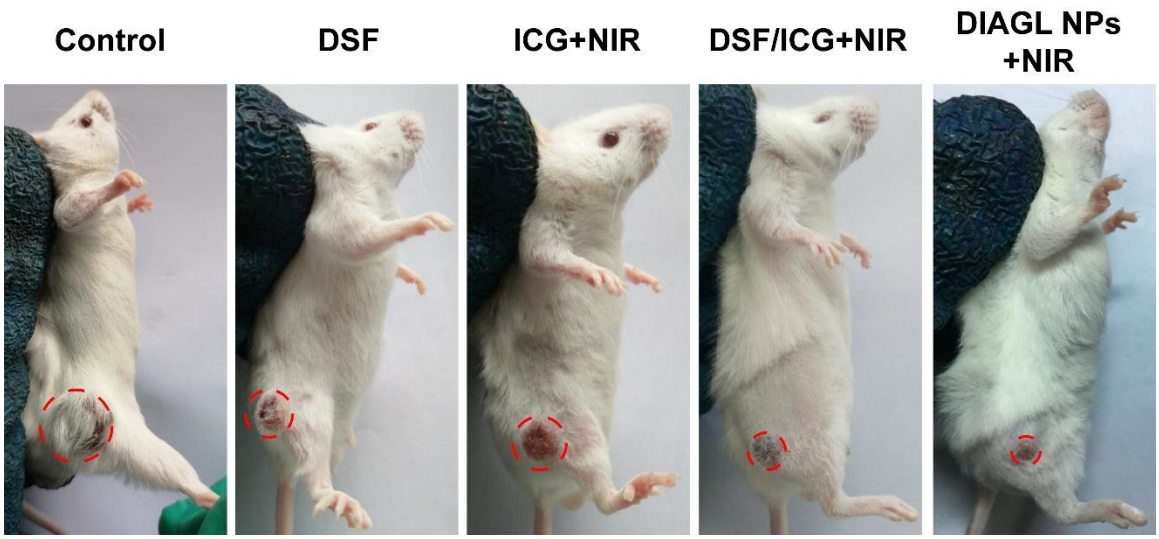

Fig. S19. Representative photos of xenografted mice on 21 days after treatments. The tumors were marked with red circles and their size.

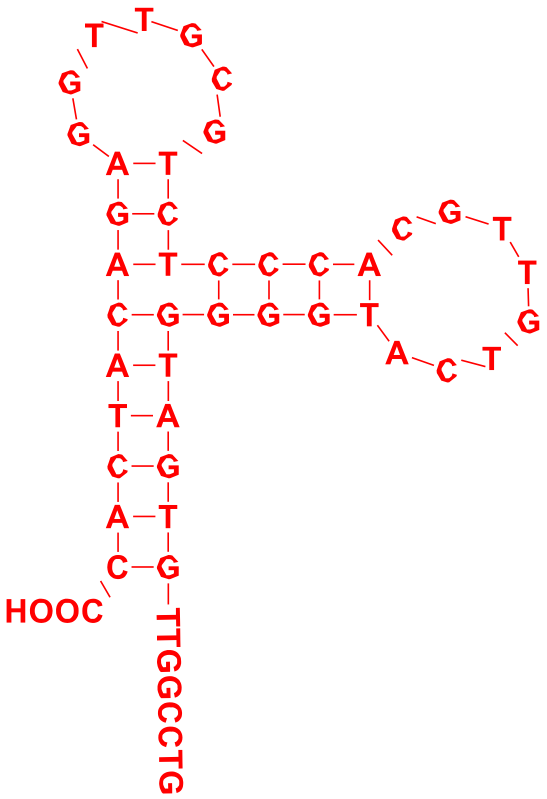

Fig. S20. Anti-EpCAM aptamer sequence and structure. The deoxyribonucleotide sequence Anti-EpCAM aptamer (5'COOH- CAC TAC AGA GGT TGC GTC TGT CCC ACG TTG TCA TGG GGG GTT GGC CTG-3').